

GT2011-458-)

EXPERIMENTS ON AFT-DISK CAVITY INGESTION IN A MODEL 1.5-STAGE AXIAL-FLOW TURBINE

J. Balasubramanian, N. Junnarkar, D.W. Zhou,
 R.P. Roy
 Arizona State University
 Mechanical and Aerospace Engineering
 Tempe, AZ 85287, USA

Y.W. Kim, H.K. Moon
 Solar Turbines Incorporated
 San Diego, CA, USA

ABSTRACT

Experiments were carried out in a model 1.5-stage (vane-blade-vane) axial-flow air turbine to investigate the ingestion of main-stream air into the aft disk cavity. This cavity features rotor and stator rim seals with radial clearance and axial overlap, and an inner labyrinth seal. Results are reported for two main air flow rates, two rotor speeds, and three purge (secondary) air flow rates. The initial step at each experimental condition was the measurement of time-average static pressure distribution in the turbine stage to ensure that a nominally steady run condition had been achieved. Subsequently, tracer gas concentration and particle image velocimetry (PIV) techniques were employed to measure, respectively, the main gas ingestion into the disk cavity (rim and inner parts) and the fluid velocity field in the rim cavity. Finally, the egress trajectory of the purge air into the main-stream air was mapped in the axial-radial plane by PIV at multiple circumferential positions within one aft vane pitch. The purge air egress trajectory and velocity field are important because the interaction of this air with the main gas stream has aerodynamic, stage performance, and downstream vane/endwall heat transfer implications.

NOMENCLATURE

b outer radius of disk cavity- Fig. 1
 C CO₂ gas concentration
 C_{vax} vane axial chord length
 cfm cubic feet per minute
 C_{p,max} pressure coefficient characterizing the pressure asymmetry in the annulus
 C_w dimensionless mass flow rate of purge air, = $\dot{m}_{\text{purge}}/\mu b$
 C_{w, fd} dimensionless free disk pumping mass flow rate, = $0.219\text{Re}_\phi^{0.8}$
 C_{w,min} minimum purge air flow rate required to prevent ingestion

dT time between laser pulse pair
 G_c seal-clearance ratio (s_c/b)
 K empirical constant in evaluating C_{w,min}
 \dot{m} mass flow rate of air (kg/s)
 r radial coordinate
 \underline{r} position vector
 s_c rim seal axial clearance
 Re_{vax} main air flow Reynolds number, = $\rho V_{\text{ax}} C_{\text{vax}} / \mu$
 Re_φ disk rotational Reynolds number, = $\rho \Omega b^2 / \mu$
 rpm revolutions per minute
 U(r) local rotor disk speed (m/s) , = Ωr
 V_{ax} mixed-mean axial velocity of main air in annulus
 V_r(r) local radial velocity of air (m/s)
 V_φ(r) local tangential velocity of air (m/s)
 Δp_{max} peak-to-peak amplitude of circumferential pressure assymetry
 x axial coordinate, measured upstream from the aft vane leading edge
 β₂ angle, to axial direction downstream, of the main air velocity relative to the blade – at just downstream of front vane trailing edge (°)
 η sealing effectiveness
 μ dynamic viscosity of air (kg/m/s)
 ρ density of air (kg/m³)
 Φ azimuthal coordinate
 Ω rotor speed

Subscripts

amb ambient
 main main air
 purge purge air

INTRODUCTION

Ingestion of hot mainstream gas into the rotor-stator disk cavities of a gas turbine is a well-known phenomenon.

This affects the durability of cavity internals, especially that of the rotor disk. To counter ingestion, the rotor and stator disks are provided with rim seals; additionally, purge air bled from the compressor discharge is injected into the cavity. The fluid flow field in the disk cavity and the interaction of the egressing purge air with main gas are important issues. A number of studies, experimental and computational, have been performed in the past to understand these. A few selected works, mostly dealing with 1.5-stage turbine setups, are discussed in the following.

Bohn *et al.* [1] carried out unsteady two-dimensional laser Doppler velocimetry measurements in the front cavity of a 1.5-stage axial flow turbine featuring 16 vanes in each vane row and 32 blades for several purge air flow rates. The flow field in the cavity was found to be influenced by the interaction of rotor blade pressure field and the stator vane wakes. The region of main gas ingestion rotated with the rotor blade; it was also observed that a reduction in purge air flow rate increased main gas ingestion. Cao *et al.* [2] reported a combined computational (CFD) and experimental study of the interaction between the mainstream air path and the purge air flow in a two-stage axial turbine for the cavity formed between the stage-2 rotor disk and the upstream stator diaphragm. A simple axial gap existed between the rotor and stator without any rim seals. Fast response pressure transducers were installed in the disk/diaphragm space to measure the unsteady pressure. Unsteady, three-dimensional CFD simulation (360 deg. azimuthal domain) of the flow in the cavity without vanes and blades present was also reported. Alternating regions of ingestion and egress that rotated at 90-97 percent of the rotor speed were found near the rim cavity.

Jakoby *et al.* [3] performed numerical simulations on a 1.5-stage model gas turbine with axial seal (a seal lip at the periphery at either side) but no radial or axial overlap. The special focus of this study was to find large-scale rotating structures in the front cavity which could cause ingestion. This phenomenon was captured by an unsteady calculation using the full 360 deg. azimuthal domain. A large-scale rotating structure that revolved with 80 percent of the rotor speed was detected in the front rim cavity when the purge flow rate fell below a certain limit. This structure significantly influenced the ingestion of mainstream gas into the front cavity. Bohn *et al.* [4] carried out experiments to study the influence of rim seal geometry on the ingestion of main air into the front cavity of a 1.5-stage axial turbine. Two seal configurations were: an axial seal (with seal lip at periphery on both the rotor and stator) and a radial seal. Tracer gas concentration and static pressure measurements were obtained in the cavity. The radial seal configuration was found to perform with a much higher efficiency than the axial seal. Rabs *et al.* [5] performed CFD analysis on the front cavity of a 1.5-stage gas turbine derived from [4] to investigate the influence of Kelvin-Helmholtz vortices near the rim seal on ingestion of main gas into the disk cavity. A 22.5 deg sector was simulated. Connection between the vortex structure and main gas ingestion/purge gas egress was discussed.

Gallier *et al.* [6] mapped, by particle image velocimetry, the instantaneous velocity field in an axial-radial plane encompassing the main gas path and the rim seal region of a turbine stage. Ten blade positions relative to the mapping plane were recorded, this characterizing the effect of the rotor potential field on ingestion, egress, and secondary flow structure in the main gas path. McLean *et al.* [7] conducted experiments to study the influence of purge air outflow into the main gas path on the aerodynamics and performance of a turbine stage. Bohn *et al.* [8] presented a correlation for estimating the minimum cooling air required to prevent ingestion into a disk cavity in terms of main gas pressure variations and rim seal geometry.

Huning [9] developed a new parametric single gap turbine rim seal model to predict the main gas ingestion into the disk cavity. The model results were compared with published experimental results. Owen *et al.* [10] solved the orifice equations and obtained values for the case of externally induced ingress and the combined ingress cases.

In the present paper, our main objectives were to study the ingestion of main gas into the aft-disk cavity (rim, inner) of a 1.5-stage model air turbine and the manner in which the purge air egressed from the same cavity into the main gas path. Static pressure measurements, tracer gas measurements, and particle image velocimetry were employed in the measurements.

EXPERIMENTAL APPARATUS

The 1.5-stage (vane-blade-vane) model axial-flow air turbine used in this work is shown in Fig. 1. The 403.2 mm diameter (part plexiglass, part aluminium) rotor disk has 52 partial-height and partial-length blades. There are 59 partial-height and full length vanes in the front vane row and the aft vane row. The blade and vane heights are such that given the main blower capacity, sufficiently high main air stream-wise velocity can be obtained so as to result in an acceptable velocity triangle upstream of the blade row at prescribed rotor speeds. The front vanes turn the incoming air by 60.1 degrees. Rim seals are present on both the rotor and stator disks. Purge air is injected at the hub of the aft disk cavity as shown in Fig 1a. Additionally, the aft disk cavity contains an inner labyrinth seal which essentially divides the cavity into an inner cavity and an outer (rim) cavity. The rim cavity is optically accessible from both the radial and axial directions. Table 1 lists the important dimensions of the rim and labyrinth seals.

The main air and the purge air are supplied by separate centrifugal air blowers equipped with variable-frequency motor drives. The main air flow rate is measured by a calibrated pitot tube rake located in the blower suction duct; the purge air flow rate is measured by a turbine flow meter. The rotor speed is controlled by an adjustable frequency drive equipped with a dynamic braking resistor.

Table.1 Salient features of the seals

s_c (rim seal axial clearance)	6.05 mm
s (disk cavity gap)	18.75 mm
b (disk cavity radius)	196.5 mm
$G_c = s_c/b$	0.0308
rim seal radial clearance	2.6 mm
rim seal axial overlap	6.6 mm
labyrinth seal radial clearance	0.75 mm

Static pressure measurement

A differential pressure transducer (Validyne)-digital manometer (Validyne) - Scanivalve set-up was used to measure the time-average static gage pressure distribution in the aft disk cavity (both rim and inner cavities) at the stator, and the axial-circumferential pressure distributions in the main air path. Pressure taps were provided on the stator disk at seven radial locations, Fig 1a. In the main air path, pressure was measured at the outer shroud over two vane pitches using seventeen azimuthally equally spaced pressure taps at each of four axial positions (Fig 1b). Additionally, four pressure taps spaced equally over one vane pitch at $r=199$ mm on the stator disk measured the circumferential variation of static gage pressure near the rim.

The uncertainty in the measured pressure, estimated on the basis of instrument and data acquisition uncertainties, is ± 2 percent of the static gage pressure.

Ingestion of mainstream air

To measure ingestion into the aft disk cavity, the purge air was seeded with carbon dioxide as the tracer gas. The CO_2 volumetric concentration in the purge air was monitored just upstream of its entry into the cavity and maintained at 4.0 percent. Radial locations of the concentration taps were the same as those of the pressure taps on the stator disk. The CO_2 concentration in the main air was also monitored upstream of the front vanes to serve as reference in the sealing effectiveness (η) calculation.

The CO_2 concentration in the gas sample was measured by an NDIR gas analyzer (Siemens – Ultramat). The uncertainty in the measured CO_2 percent volumetric concentration is ± 0.11 percent.

The time required for measuring tracer gas concentration is long and hence, the measured ingestion of main air into the cavity is a time-average value over many rotor revolutions. It is, however, local with respect to the vane positions and the radial coordinate.

Air velocity vector maps – aft disk cavity

A dual Nd:YAG laser (Spectra-Physics PIV-200) provided short pulses (≈ 10 ns width) of 532 nm (green) light to illuminate the seed particles (olive oil droplets, 1-2 μm , mixed with the purge air) in the rim cavity air flow. The light sheet was introduced through the polished plexiglass outer shroud and could be accurately positioned by means of a three-

dimensional traverse equipped with a rotary stage. The four axial (x) positions of the radial-azimuthal plane where images were obtained in the rim cavity are shown by green vertical lines in Fig 1a. The plane of the laser sheet is normal to the plane of paper.

The images were captured with a high-resolution CCD camera (2048×2048 pixels). The camera was mounted on a three-dimensional traverse for positioning.

Purge air egress velocity vector maps

The trajectory of the purge air flowing out of the aft disk cavity into the main air stream in the region between the blade trailing edge and the aft vane leading edge was mapped in the axial-radial plane using PIV. The laser sheet was introduced radially inward through the outer shroud. The plane of the laser sheet (shaded yellow in Fig. 1) is parallel to the plane of paper, and the camera, with its axis normal to the plane of the laser sheet, imaged the field of view (FOV, 26.13 mm \times 26.13 mm) indicated by a blue rectangle, Fig. 1, through the curved plexiglass outer-shroud. As such, the image seen by the camera contained distortion due to light ray refraction. This distortion is along the radial co-ordinate only and is non-uniform because of varying outer shroud thickness that rays from different points across the FOV (along the radial coordinate) passed through. A mapping algorithm similar to one developed in [11] was employed to correct each image before cross-correlation to obtain velocity vectors.

Figure 12 shows two circumferential positions within one vane pitch, AA, where the purge air egress velocity vector maps were obtained. The locations correspond to 1/3rd vane pitch and vane leading edge. All instantaneous images were obtained at the same juxtaposition of the vanes and blades so that ensemble-averaged maps could be constructed.

RESULTS AND DISCUSSIONS

Experiments performed

Experiments were carried out for the conditions listed in Table 2. In Expt. Set II, both the rotor speed and main air flow rates are higher compared to Expt. Set I. This is because we aimed to maintain the angle β_2 (see Nomenclature) in the main air velocity triangle downstream of the front vane row (Fig 1b) the same for both sets since this velocity triangle may influence the ingestion process [12]. This, on the other hand, meant that the effect of either the rotor speed or the main air flow rate on the parameters of interest could not be isolated from the data.

The static pressure measurements and the main air ingestion measurements were performed for all conditions listed in Table 2. The PIV measurements were performed for only the purge air flow rates that are shown in bold letters. The PIV measurements were not performed at the lowest purge air flow rate since at that flow rate, adequate seed droplets could not be delivered into the imaged regions.

Table 2 Experimental Conditions

Expt. Set No.	Main air flow rate (Re_{vax})	Rotor speed (Re_ϕ)	Purge air flow rate (c_w)	β_2 ($^\circ$)	Free disk pumping flow rate ($c_{w,fd}$)
I	6.67×10^4	4.93×10^5	820	35.0	7840
			1640		
			2470		
			3290		
II	7.12×10^4	5.26×10^5	820	35.0	8260
			1640		
			2470		
			3290		

The average ambient pressure during the experiments was 97.3 kPa (absolute) and the average ambient temperature was 23.5 °C. The average static pressure of the mainstream air at front vane inlet was 96.2 kPa (absolute) and that of the purge air at the aft disk cavity entry was 96.6 kPa (absolute). The latter two pressures changed slightly as the main and purge air flow rates were changed. The calculated Mach number for the main air in the annulus for Expt Set II is 0.12, this being much smaller compared to actual engine conditions.

The estimated uncertainties in the values of the dimensionless parameters Re_ϕ , Re_{vax} and c_w are respectively, ± 2 percent, ± 3 percent and ± 5 percent.

For brevity, only selected results are presented in the following.

Time-average static pressure

For each experimental condition, the distributions of the time-average static pressure at the main air path outer shroud and at the stator surface in the aft disk cavity were measured. These measurements helped ensure that nominally steady and, in the main air path, circumferentially periodic flow field was achieved.

Figure 2 presents, for Expt. Set II and $c_w=2470$, the circumferential distribution of static pressure at the main air path outer shroud at $0.115C_{vax}$ downstream of the front vane trailing edge plane. The static pressure varies circumferentially in a periodic manner following the vane pitch with the highest pressures occurring in the mid-region of the vane wakes. The pressure taps from #1 to #9 and #9 to #17 span the two vane pitches over which measurements were obtained.

The circumferential distribution of static pressure at the main air path outer shroud for three axial locations downstream of the rotor blade trailing edge plane, and at $r/b=1.013$ of the aft cavity stator surface are presented in Fig. 3 for the same experiment. The pressure distributions in the main air path are circumferentially periodic following the vane pitch (both front and aft); they also shift in phase along the stream-wise direction. The strength of circumferential asymmetry in pressure decreases from the $0.115C_{vax}$ axial location to the $0.307C_{vax}$ location. It, however, increases at the $0.538C_{vax}$ location quite possibly because of the purge air mixing with the

main air in the region and because of the proximity of the aft vanes. That the peaks of the pressure distributions move toward the aft vane leading edges as the vanes are approached should also be noted. One other feature of these pressure distributions is: there is a discernible positive slope in the average static pressure in the direction of rotation for each distribution (this was the case for all other experiments as well). An explanation is not offered at this juncture.

The radial distributions of static pressure within the aft disk cavity, at the stator disk, for Expt. Set II are shown in Fig. 4a. In the inner cavity, the static pressure increases radially and then decreases across the labyrinth seal. In the rim cavity, the static pressure increases radially and then decreases across the stator rim seal. For comparison, the radial distribution of static pressure at the stator for $c_w=2470$ along with 'equivalent dynamic pressure ($\rho V_\phi^2/2$)' due to fluid tangential velocity (rotation) in the rim cavity are plotted in Fig 4b. The fluid tangential velocity at $x/s=0.267$ (see Fig. 8) is used to evaluate the equivalent dynamic pressure. The static pressure at the stator and the equivalent dynamic pressure increase by approximately the same amount radially across the rim cavity.

Mainstream air ingestion measurements

Figure 5a shows the radial distribution of local sealing effectiveness on the aft disk cavity stator surface for Expt. Set II. The effectiveness is defined as

$$\eta(r) = \frac{c(r) - c_{main}}{c_{purge} - c_{main}} \quad (1)$$

The local sealing effectiveness demonstrates the well-known trend of increasing as the purge air flow rate increases. The distribution of sealing effectiveness within the inner cavity is flat. For the highest purge air flow rates ($c_w = 3290$), the inner cavity is effectively sealed off from main air ingestion. A steep drop in η occurs across the labyrinth seal for all purge air flow rates and significant ingestion into the rim cavity takes place. The purge air exits the labyrinth seal as a jet-like flow that impedes the rim cavity fluid from entering the inner cavity. In other words, the ingested main air stays predominantly in the rim cavity before getting ejected into the main air path.

At the lower purge air flow rates, there is some ingestion of main air into the inner cavity as well. The curtain of fluid formed by the jet is apparently inadequate in sealing the inner cavity now.

The circumferential variation of sealing effectiveness was measured at the stator surface over one vane pitch at $r/b = 1.013$. No significant azimuthal variation in the value of η was found from these measurements.

It was also observed that compared to Expt. Set I the ingestion of main air was higher in Expt. Set II. The latter featured higher main air flow rate as well as higher rotor speed at the same purge air flow rates.

Fig 5b shows the variation of η with C_w for Expt Set II at $r/b = 0.679$, this being in the inner cavity just inboard of the labyrinth seal. It is observed that *in the inner cavity* the effectiveness tends to unity as C_w reaches to a value of about 3300. The correlation given in [8] for a generic disk cavity (i.e., one not subdivided into a rim cavity and an inner cavity) is

$$C_{w,min} = \pi K G_c Re_w \sqrt{0.5 C_{p,max}} \quad (2)$$

where

$$C_{p,max} = \Delta p_{max} / 0.5 \rho V_{ax}^2 \quad (3)$$

Using a value of 0.2 for the empirical constant K results in $C_{w,min} = 6250$. If we consider ingestion into the *rim cavity* only, Fig. 5a, it is doubtful that the sealing effectiveness will approach unity at such a value.

Aft rim cavity fluid velocity field

Velocity vector maps were obtained over one quadrant of the rim cavity for the highlighted experimental conditions in Table 2. At each experimental condition, the velocity vector maps were obtained at four axial positions, viz., $x/s = 0.267, 0.517, 0.587, 0.792$. Ten instantaneous vector maps were obtained at each position; the corresponding ensemble-averaged map was constructed from the ten maps.

Figures 6 and 7 show respectively, for Expt. Set II, $c_w = 2470$, the ensemble-averaged velocity vectors in the $r-\Phi$ plane at $x/s = 0.267$ and 0.792 . In the images, the region between the dashed circular lines denotes the rim cavity.

Figure 8 and 9 contain, respectively, the non-dimensionalized circumferential-average fluid tangential velocity $V_\phi(r)/U(r)$, and radial velocity $V_r(r)/U(r)$ as determined from the maps in Figs. 6 and 7. The tangential velocity is the highest at the axial position near the rotor and the lowest at the position close to the stator. Additionally, near the rotor, the tangential velocity remains almost constant over 60 percent of the radial extent of the rim cavity before increasing sharply in the outer region.

Figure 9 shows that the fluid radial velocity is very low in the rim cavity except near the rotor. This can be attributed to the cavity 'core region' where the fluid velocity is primarily tangential. The radial velocity is directed outwards near the rotor, a combined effect of disk pumping and the purge

air flow. At the other axial positions, the radial velocity is mostly directed radially inward; this could be due to the combined effect of the re-circulation of cavity air and the inward flow of ingested main air.

Figure 10 and 11 show, respectively, the non-dimensionalized fluid tangential and radial velocities over two 2-degree sectors, obtained from an instantaneous velocity vector map for Expt. Set II, $c_w = 2470$ at $x/s = 0.792$. Comparing Figs. 11 and 9, it is seen that there are large fluctuations in the fluid instantaneous radial velocity; these get smeared out in the ensemble-averaging process. Circumferentially there are sub-sectors where the radial velocity is predominantly negative (i.e. fluid flowing radially inward) and predominantly positive (i.e. fluid flowing radially outward). The fluid instantaneous tangential velocity plot, Fig. 10, has a much-compressed scale; as such, the fluctuations are not as apparent.

Purge air egress trajectory and velocity field

The purge air egress trajectory/velocity maps were obtained for the highlighted experimental conditions in Table 2. The selected maps presented here are all ensemble-average maps, each an average of five instantaneous maps. The maps shown correspond to two circumferential positions within one aft vane pitch AA as shown in Fig 12.

Figures 13 and 14 show the maps for Expt Set II, $c_w = 2470$ at the $1/3^{\text{rd}}$ vane pitch position and at the vane leading edge position, respectively. That the egressing purge air will influence the main gas flow field in the region is apparent. This has implications for airfoil/endwall heat transfer as well as aerodynamic loss.

There are significant differences between the egress trajectories at the $1/3^{\text{rd}}$ vane pitch and vane leading edge positions. At $1/3^{\text{rd}}$ vane pitch, the purge air remains in the PIV measurement plane as it flows into the main air path whereas at the vane leading edge position, the purge air moves out of the measurement plane once it enters the main air path. A possible reason is that at the latter position the main air has to flow around the vane leading edge because of the higher pressure that develops upstream of the leading edge, this giving rise to an additional tangential movement of the air. The purge air follows suit, flowing around the vane leading edge plane and hence out of the PIV measurement plane.

Two other observations based on the results of all of the Table 2 experiments are: (i) at a particular main air flow rate, a higher purge air flow with its higher radial momentum penetrates farther into the main air path; and (ii) at the same purge air flow rate, its radial penetration into the main air path was farther in the case of Expt. Set I which had lower main air flow and thus lower main air axial momentum.

CONCLUDING REMARKS

Described in this paper were experiments in which fluid static pressure distribution, mainstream air ingestion, fluid velocity field in the aft disk cavity, and the purge air egress flow field were measured in a model 1.5-stage axial flow

turbine. The measurements were for two main air flow rates, two rotor speeds, and three-four purge air flow rates. The aft disk cavity featured an inner labyrinth seal and seals with radial clearance and axial overlap on stator and rotor disk rims.

Scrutiny of the ensemble-averaged fluid velocity vector maps in the aft rim cavity showed that the tangential velocity was higher near the rotor disk compared to near the stator. The radial velocity was low throughout the rim cavity indicating a 'core region' where the fluid velocity is predominantly tangential. In the instantaneous velocity maps, high fluctuations were seen in the radial velocity. In different circumferential sectors, the fluid radial velocity could be predominantly positive or negative.

Pressure measurements in the aft disk cavity indicated that the radial pressure gradient in the rim cavity was primarily due to the tangential motion (rotation) of the cavity fluid.

The ingestion measurements indicated that the inner cavity was completely sealed off from main gas ingestion at the highest purge air flow rate. However, significant ingestion continued to occur in the rim cavity. Ingestion was found to be higher in the higher main air flow, higher rotor speed experiments at the same purge air flow rate.

The purge air egress trajectory was found to depend on the main air and purge air flow rates, and the azimuthal position within the aft vane pitch.

ACKNOWLEDGMENTS

The authors gratefully acknowledge the support of this work by Solar Turbines Incorporated, San Diego, CA.

REFERENCES

- [1] Bohn, D. E., Decker, A., Ma, H., and Wolff, M., 2003, "Influence of Sealing Air Mass Flow on the Velocity Distribution In and Inside the Rim Seal of the Upstream Cavity of a 1.5 Stage Turbine", ASME Paper No. GT2003-38459
- [2] Cao, C., Chew, W. J., Millington, R. P., and Hogg, I. S., 2003, "Interaction of Rim Seal and Annulus Flows in an Axial Flow Turbine", ASME Paper No. GT2003-38368
- [3] Jakoby, R., Zierer, T., Klas, L., and Larsson, J., deVito, L., Bohn, E. D., Funcke, J and Decker, A., 2004, "Numerical simulation of the Unsteady Flow Field in an Axial Gas Turbine Rim Seal Configuration," ASME Paper GT2004-53829
- [4] Bohn,D.E., Decker, A., and Ohlendorf, N., 2006, "Influence of Radial and Axial Rim Seal Geometry on Hot Gas Ingestion into the Upstream Cavity of a 1.5 Stage Turbine", ASME Paper No. GT2006-90453
- [5] Rabs, M., Benra, A. F., Dohmen, J. H., and Schneider, O., 2009, "Investigation of Flow Instabilities near the Rim Cavity of a 1.5 Stage Gas Turbine", ASME Paper No. GT2009-59965
- [6] Gallier, D.K., Lawless, B.P., and Fleeter, S., 2000, "Investigation of Seal Purge flow Effects on the Hub Flow Field in a Turbine Stage using Particle Image Velocimetry", AIAA Paper 2000-3370
- [7] McLean, C., Camci, G., and Glezer, B., 2001, "Mainstream Aerodynamic Effects Due to Wheelspace Coolant Injection in a High-Pressure Turbine Stage: Part I: Aerodynamic Measurements in the Stationary Frame", ASME J. Turbomach., 123(4), pp. 687-696
- [8] Bohn, D. and Wolff, M., 2003, "Improved Formulation to Determine Minimum Sealing Flow – $C_{w,min}$ - for Different Sealing Configuration", ASME Paper GT2003-38465
- [9] Huning, M., 2010, "Parametric Single Gap Turbine Rim Seal Model With Boundary Generation For Asymmetric External Flow", ASME Paper GT2010-22434
- [10] Owen, J.M., Zhou, K., Wilson, M., Pountey, O., and Lock, G., 2010, "Prediction of Ingress Through Turbine Rim Seals. Part I: Externally-Induced Ingress", ASME Paper GT2010-23346
- [11] Murphy, M.J., 2009, "Development of an Ultra-High Speed Dynamic Witness-Plate Particle Image Velocimetry for Micro Detonator Study", Ph.D. Thesis, Arizona State University.
- [12] Roy, R.P., Feng, J., Narzary, D., and Paolillo, R. E., 2005, "Experiments on Gas Ingestion Through Axial-Flow Turbine Rim Seals," ASME J. Engineering for Gas Turbines and Power, Vol. 127, pp. 573-582.

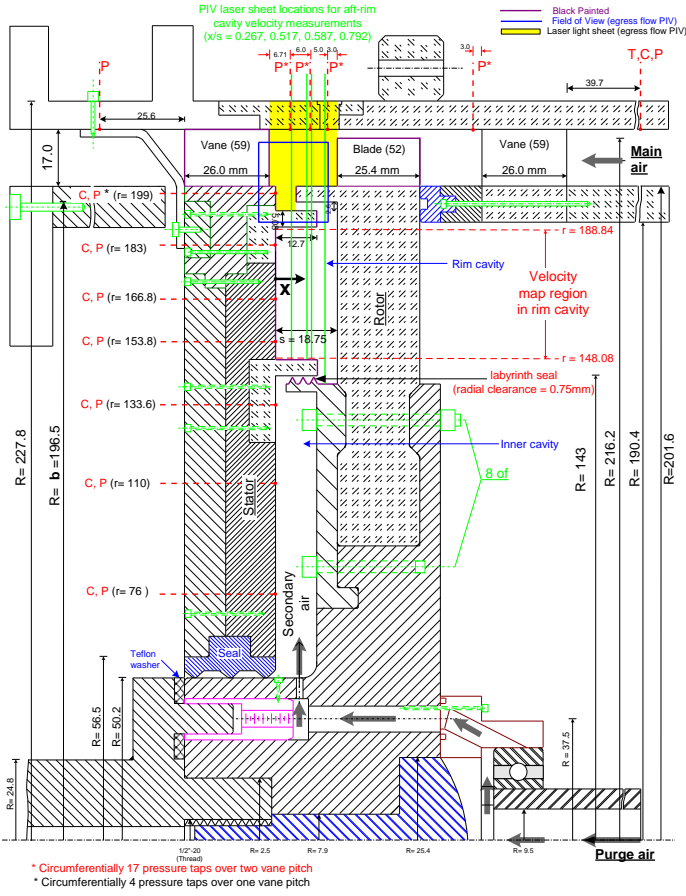


Fig.1a Schematic diagram of the 1.5-stage turbine (C: gas concentration tap, P: static pressure tap; T: thermocouple); the yellow shaded region is mapped by PIV for the egress flow PIV measurement. The overlaid blue rectangle represents the FOV. All dimensions are in mm.

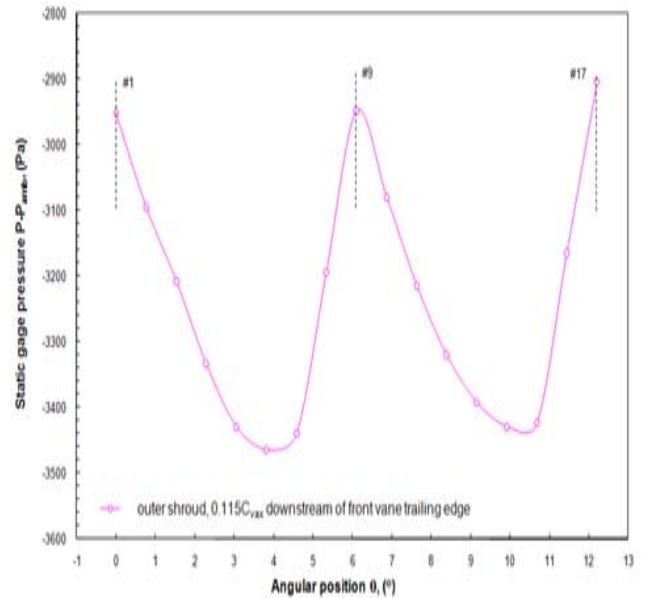


Fig.2 Circumferential variation of time-average static pressure in the main air path outer shroud at 0.115 C_{vax} downstream of front vane trailing edge — Expt. Set II, $c_w = 2470$.

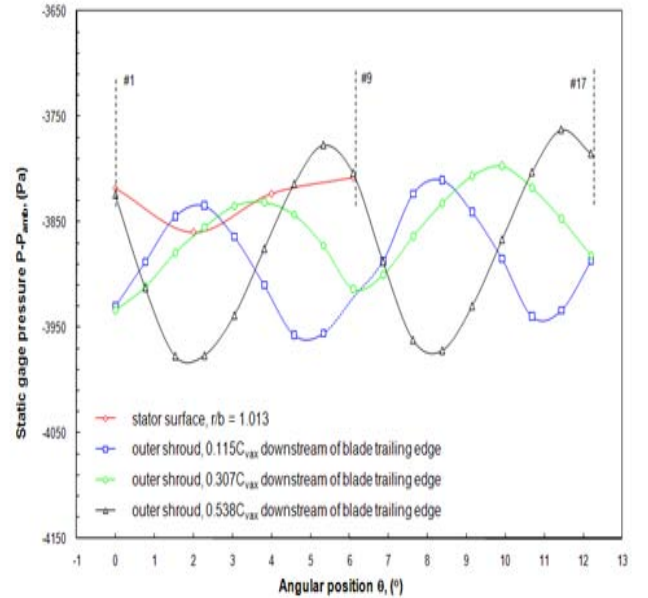


Fig.3 Circumferential variation of time-average static pressure in the main air path outer shroud at three axial locations downstream of blade trailing edge, and at the aft stator disk surface at $r/b=1.013$ — Expt. Set II, $c_w = 2470$.

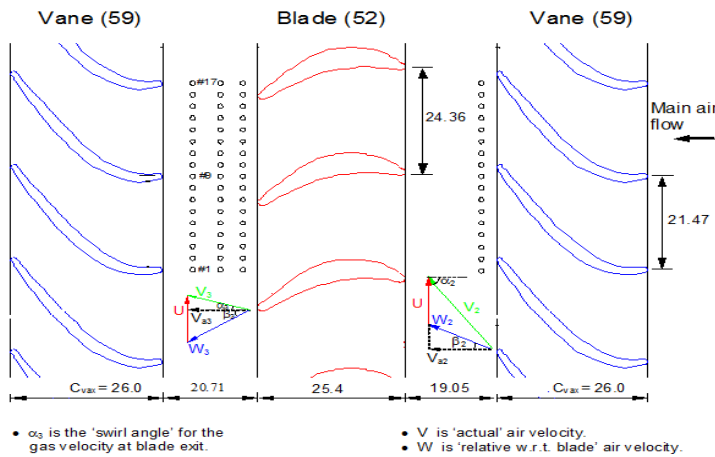


Fig.1b Pressure tap locations on the outer-shroud, in the main gas path and the velocity triangles of the main air flow at the blade inlet and outlet. All dimensions are in mm.

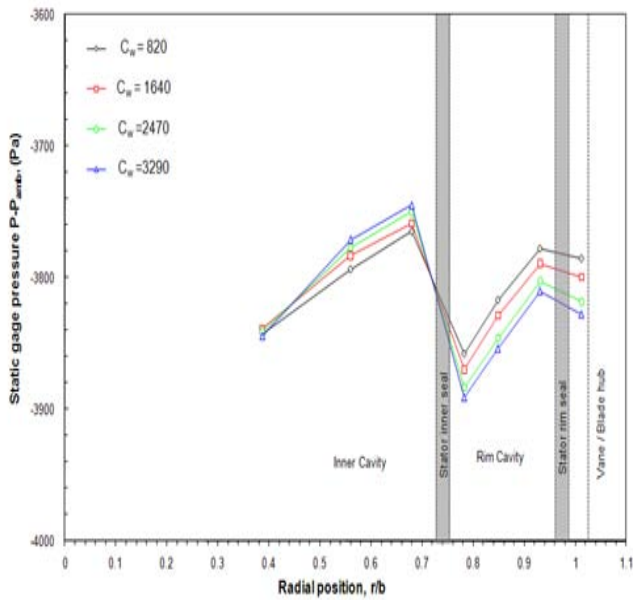


Fig.4a Radial distribution of static pressure in the aft-disk cavity at the stator surface — Expt. Set II.

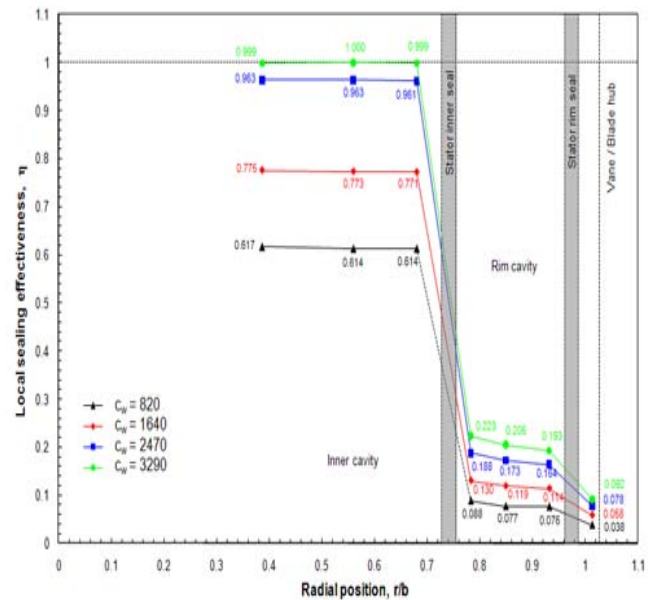


Fig.5a Effect of c_w on the radial distribution of sealing effectiveness at the stator in the aft-disk cavity — Expt. Set II

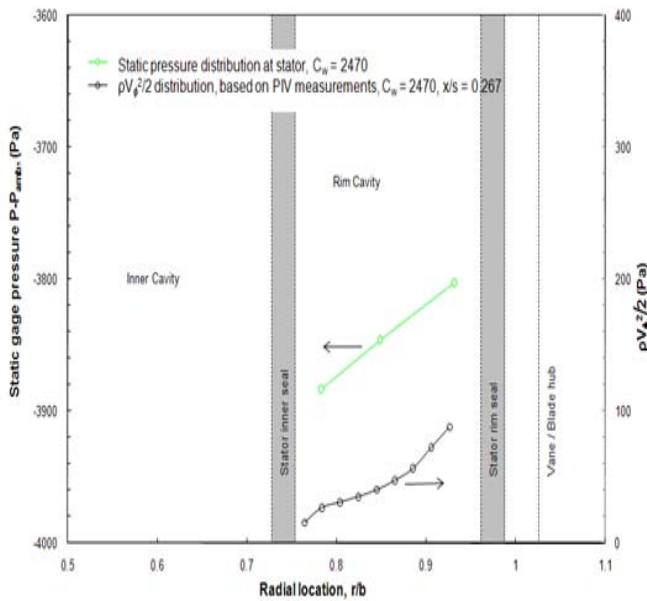


Fig.4b Comparison of static pressure at the stator surface and the 'equivalent dynamic pressure' due to fluid rotation in the aft-rim cavity. (Arrows indicate the axis to be referred for each curve)

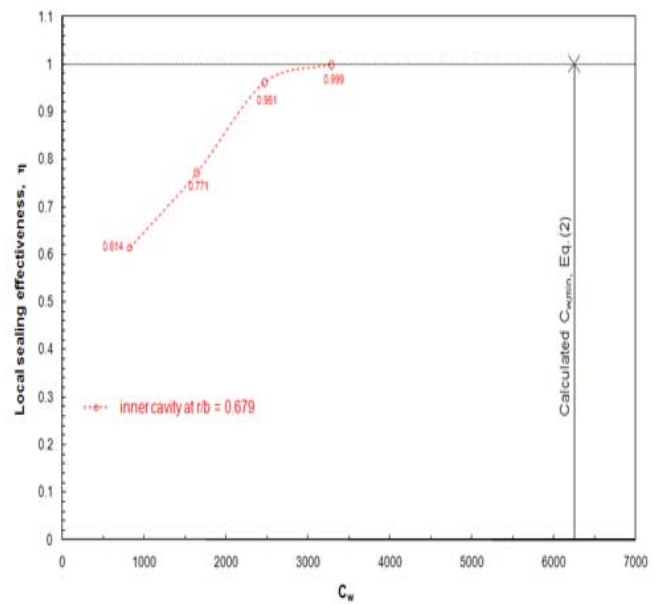


Fig.5b Variation of sealing effectiveness (η) with C_w for Expt. Set II within the inner cavity at $r/b = 0.679$

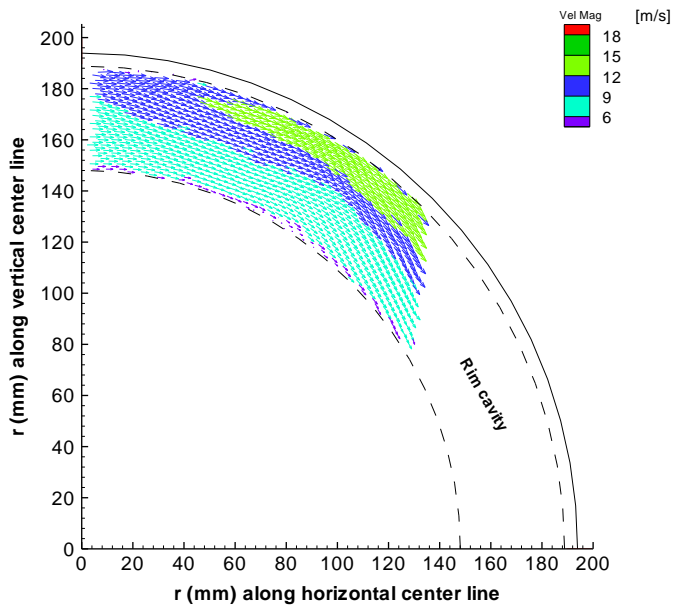


Fig.6 Ensemble-average velocity vector map in the aft-rim cavity at $x/s=0.267$ — Expt. Set II, $c_w = 2470$, $dT = 15 \mu s$.

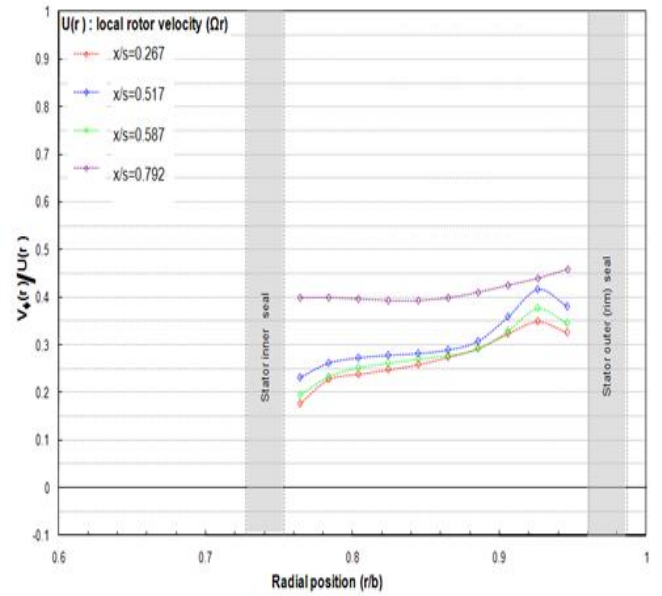


Fig.8 Fluid Circumferential-average tangential velocity from ensemble-averaged maps at the four axial locations in the rim cavity — Expt. Set II, $c_w = 2470$

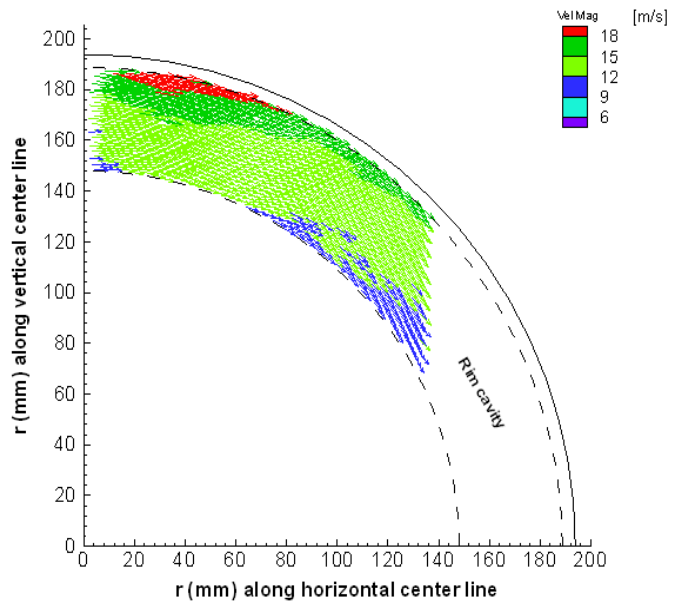


Fig.7 Ensemble-average velocity vector map in the aft-rim cavity at $x/s=0.792$ — Expt. Set II, $c_w = 2470$, $dT = 15 \mu s$.

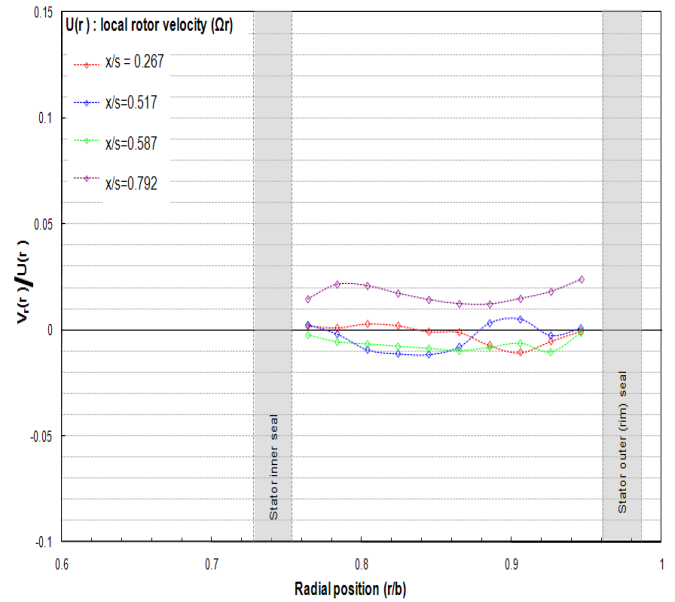


Fig.9 Fluid Circumferential-average radial velocity from ensemble-averaged maps at the four axial locations in the rim cavity — Expt. Set II, $c_w = 2470$

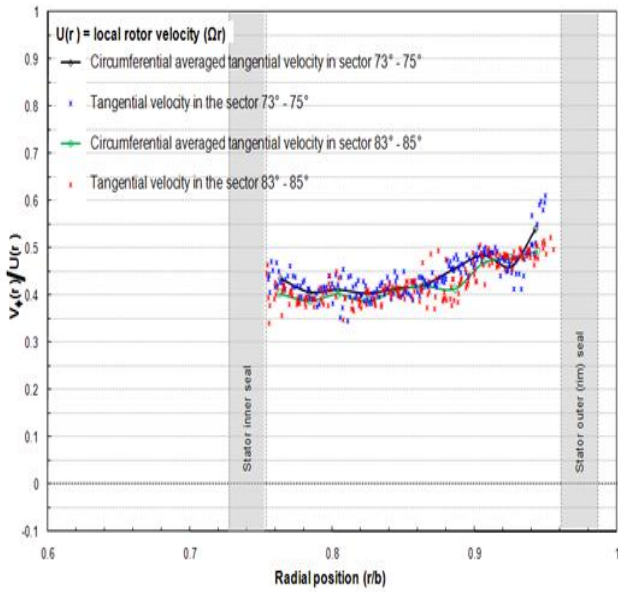


Fig.10 Fluid Instantaneous tangential velocity over two different sectors at $x/s=0.792$ — Expt. Set II, $c_w = 2470$.

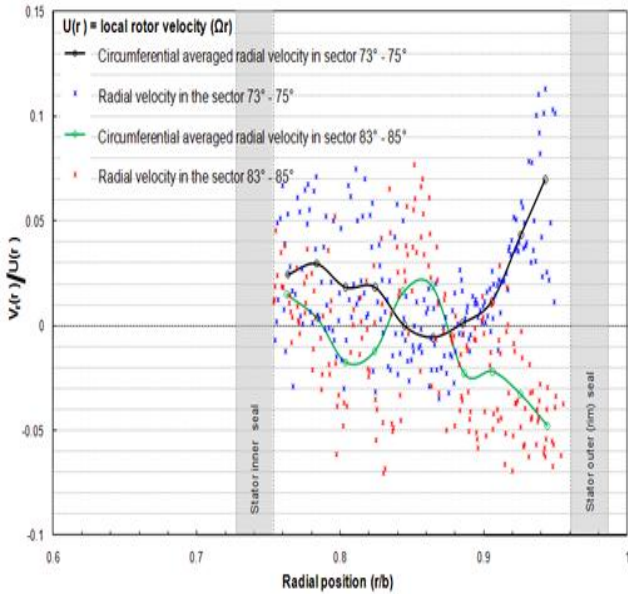


Fig.11 Fluid Instantaneous radial velocity over two different sectors at $x/s=0.792$ — Expt. Set II, $c_w = 2470$.

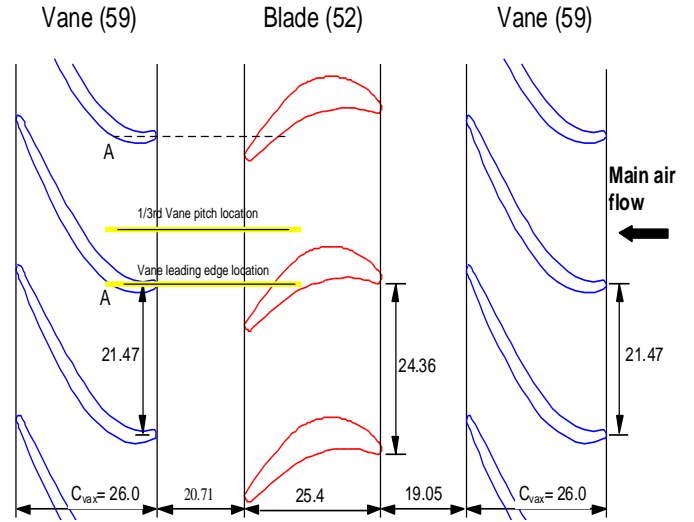


Fig.12 Relative position of vanes and blades for the purge air egress flow measurements. All PIV images were obtained within the aft-vane pitch AA. (all dimensions are in mm)

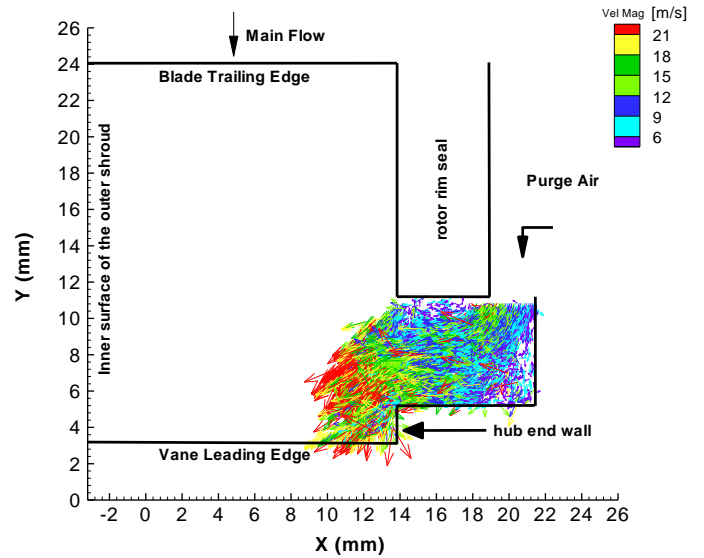


Fig.13 Ensemble-average egress air velocity map at the $1/3^{\text{rd}}$ aft-vane pitch location — Expt. Set II, $c_w = 2470$. ($\Delta T = 3.0 \mu s$)

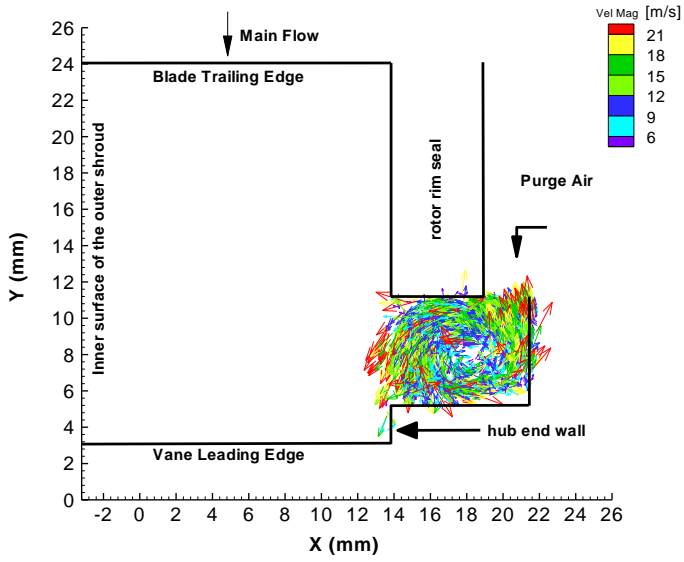


Fig.14 Ensemble-average egress air velocity map at the aft-vane leading edge location — Expt. Set II, $c_w = 2470$. ($dT = 3.0 \mu s$)